A NEW ALGORITHM FOR ASSESSING THE XCO_2 OVER PENINSULAR MALAYSIA BASED ON GOSAT DATA

SIM CHONG KEAT

UNIVERSITI SAINS MALAYSIA

2015

A NEW ALGORITHM FOR ASSESSING THE XCO_2 OVER PENINSULAR MALAYSIA BASED ON GOSAT DATA

by

SIM CHONG KEAT

Thesis submitted in fulfillment of the requirements for the degree of Doctor of Philosophy

OCTOBER 2015

ACKNOWLEDGEMENTS

I would like to express my sincere thank and gratitude to my main supervisor, Assoc. Prof. Lim Hwee San, who supervised me throughout my research. I am also thankful for his dedicated guidance, inspiration, comments, suggestions, and advice. Without Assoc. Prof. Lim Hwee San's patience, care and concern, this project would not have been completed. Assoc. Prof Lim Hwee San has been a fantastic supervisor.

I am particularly grateful to my co-supervisor Prof. Mohd. Zubir Mat Jafri for his help and support for sharing information and ideas throughout my project. I wish to express my sincere appreciation to Prof. Mohd. Zubir Mat Jafri for assistance with the data analysis and reviewing the paper that has been submitted for peer review.

Moreover, the assistance and technical support from the staff at the School of Physics, Universiti Sains Malaysia, was paramount to the success of my project, especially the assistance and cooperation of those who directly or indirectly participated from the beginning to the end of my project. Without their assistance and participation, my research would not have been smoothly conducted and finished on time.

Eventually, I would like to acknowledge the Japan Aerospace Exploration Agency (JAXA), the Ministry of the Environment (MOE) and the National Institute for Environmental Studies (NIES) for providing free GOSAT data. My appreciation goes to the AIRS staff for their generosity in sharing valuable satellite data for public access.

I am also grateful for the Ministry of Education for rewarding me with a MyPhD scholarship under the MyBrain15 program, which covered my tuition and

living expenses during the research. A special thanks goes to the Universiti Sains Malaysia for the Exploratory Research Grant Scheme (ERGS) (Grant No. 203/PFIZIK/6730051) and the Fundamental Research Grant Scheme (FRGS) (Grant No. 203/PFIZIK/6711352) which helped finance my research. Furthermore, I greatly appreciate all of my lab mates from the Engineering Physics Laboratory, who never failed in supporting, encouraging and standing by me through thick and thin.

Lastly, the constant and invaluable supports, loves, care and concerns from my dear parents, my sisters, and my bother are highly appreciated. Without their help and encouragement, I would have been unable to complete this study on time.

SIM CHONG KEAT

2015

TABLE OF CONTENTS

CHAPTER 4- RESULTS AND DISCUSSION

LIST OF TABLES

LIST OF FIGURES

LIST OF SYMBOLS

Ar	Argon
β	Beta coefficient
CH_4	Methane
CO	Carbon Monoxide
CO_2	Carbon Dioxide
H_2O vapor	Water vapor
He	Helium
N_2	Nitrogen
N_2O	Nitrous Oxide
O_2	Oxygen
O_3	Ozone
ppb	Parts Per Billion
ppbv	Parts Per Billion By Volume
ppm	Parts Per Million
ppmv	Parts Per Million By Volume
R	Correlation Coefficient
R^2	Coefficient of Determination
Wm^{-2}	Watts per Square meter
XCH_4	Column-Averaged Dry Air Mole Fraction of CH_4
XCO_2	Column-Averaged Dry Air Mole Fraction of CO_2

LIST OF ABBREVIATIONS

AIRS	Atmospheric Infrared Sounder
AMSU	Advanced Microwave Sounding Unit
AOT	Aerosol Optical Thickness
ASY	Asymmetry Parameter
BC	Black Carbon
CAI	Cloud and Aerosol Imager
CFC	Chlorofluorocarbons
CONTRAIL	Comprehensive Observation Network for Trace gases by Airliner
EOS	Earth Observing System
FOV	Field of View
FTS	Fourier Transform Spectrometer
g-b FTS	Ground-Based High-Resolution Fourier Transform Spectrometers
GHG	Greenhouse Gas
GOSAT	Greenhouse Gases Observing Satellite
GOSAT DHF	GOSAT Data Handling Facility
GUIG	GOSAT User Interface Gateway
HDF	Hierarchical Data Format
He	Helium
HSB	Humidity Sounder for Brazil
IASI	Infrared Atmospheric Sounding Interferometer
IAV	Interannual Variations
IPCC	Intergovernmental Panel on Climate Change
ITCZ	Inter-Tropical Convergence Zone
JAXA	Japan Aerospace eXploration Agency
JPL	Jet Propulsion Laboratory
LPS	Large Point Sources
MAPE	Mean Absolute Percentage Errors
MMD	Malaysia Meteorological Department
MLR	Multiple Linear Regression
MOE	Ministry of the Environment (Japan)
MS-Excel	Microsoft Excel
NASA	National Aeronautics and Space Administration
NDVI	Normalised Difference Vegetation Index
NEE	Net Ecosystem Exchange
NEM	Northeast Monsoon
NIES	National Institute for Environmental Studies (Japan)
NIES TM	National Institute for Environmental Studies offline tracer Transport Model
NIR	Near-Infrared
NOAA	National Oceanic and Atmospheric Administration
OCO-2	Orbiting Carbon Observatory
PCs	Principal Components
PC1	Principal Component One
PC2	Principal Component Two
PCA	Principal Component Analysis
PCR	Principal Component Regression

PPDF	Photon Path Length Probability Density Function
RMSE	Root-Mean-Square Error
SCIAMACHY	Scanning Imaging Absorption Spectrometer For Atmospheric Chartography (Germany)
SO	Southern Oscillation
SSA	Single Scattering Albedo
SWIR	Shortwave Infrared
SWM	Southwest Monsoon
SPSS	Statistical Package for Social Sciences
TOA	Top of Atmosphere
TANSO	Thermal and Near-infrared Sensor for Carbon Observation (Japan)
TCCON	Total Carbon Column Observing Network
TES	Tropospheric Emission Spectrometer
TIR	Thermal Infrared
UV	Ultraviolet
VIF	Variance Inflation Factor

LIST OF PUBLICATION

1 Sim Chong Keat, Beh Boon Chun, Lim Hwee San and Mohd Zubir Mat Jafri, 2014, Multiple regression analysis in modelling of carbon dioxide emissions by energy consumption use in Malaysia, Proceeding of the National Physics Conference (PERFIK 2014), Sunway Resort Hotel and Spa, Kuala Lumpur, Malaysia. AIP Conference Proceedings 1657, 050005 (2015); Digital Object Identifier: 10.1063/1.4915185.

2 Beh Boon Chun, Sim Chong Keat, Saumi Syahreza, Mohd Zubir Mat Jafri and Lim Hwee San, 2014, Discrimination of Mangrove Species in Matang Mangrove Forest Reserve, Perak using In-situ Measurement of Hyperspectral Leaf Reflectance, Proceeding of the National Physics Conference (PERFIK 2014), Sunway Resort Hotel and Spa, Kuala Lumpur, Malaysia. AIP Conference Proceedings 1657, 110004 (2015); Digital Object Identifier: 10.1063/1.4915223

3 Sim Chong Keat, Lim Hwee San and Mohd Zubir Mat Jafri, 2015, Predicting Column Averaged Dry-Air Mole Fractions of Carbon dioxide (XCO_2) in Peninsular Malaysia by Using GOSAT Data, Proceeding of the 2013 IEEE International Conference on Space Science and Communication (IconSpace2015), Langkawi, Malaysia

4 Tan Chun Ho, Sim Chong Keat, Mohd Zubir Mat Jafri and Lim Hwee San, 2015, A Prediction Model for CO_2 Emission From Manufacturing Industry and Construction in Malaysia, Proceeding of the 2013 IEEE International Conference on Space Science and Communication (IconSpace2015), Langkawi, Malaysia.

5 C. K. Sim, H. S. Lim, and M. Z. Mat Jafri 2015 Investigation variation of carbon dioxide based on GOSAT data in peninsular Malaysia, Proceeding of the SPIE Asia-Pacific Remote Sensing Symposium, Toulouse, France.

ALGORITMA BARU UNTUK MENILAI XCO_2 BAGI SEMENANJUNG MALAYSIA BERDASARKAN DATA GOSAT

ABSTRAK

Peningkatan kepekatan karbon dioksida (CO_2) yang disebabkan oleh aktiviti antropogenik telah menjadi tumpuan banyak kajian kerana kesan buruk pemanasan global dan perubahan iklim terhadap alam sekitar. Sebagai sebahagian daripada langkah-langkah penting untuk mencapai persekitaran yang sihat, kajian pengangkutan, pengagihan dan kawasan sumber CO_2 ke negara ini adalah diperlukan. Tujuan utama kajian ini adalah untuk membangunkan satu algoritma untuk mengira "Column-Averaged Dry Air Mole Fraction of Carbon Dioxide" (XCO_2) di Semenanjung Malaysia. Empat algoritma regresi ditandakan sebagai XCO_2 NEM, XCO2 SWM, PCA1 (XCO_2 musim NEM) dan PCA2 (XCO_2 musim SWM) telah dibangunkan dengan menggunakan kaedah statistik berdasarkan Greenhouse Gases Observing Satellite (GOSAT) data. Di samping itu, kajian ini bertujuan untuk menganalisis dan mengkaji kesan pembolehubah atmosfera terpilih dengan data XCO_2. Kaedah analisis yang berbeza termasuk Regresi Linear Berganda (MLR) dan Komponen Regresi Utama (PCR) telah digunakan untuk set data GOSAT. Analisis selanjutnya telah dijalankan pada musim tengkujuh yang berbeza untuk mencapai objektif kajian. Perisian SPSS telah dijalankan untuk menguji prestasi kaedah MLR dan kaedah PCR dari segi sisihan punca kuasa dua min (RMSE). Keputusan menunjukkan bahawa persamaan regresi XCO_2 menggunakan kaedah MLR mempunyai korelasi yang tinggi dengan pembolehubah atmosfera untuk musim NEM ($R = 0.826$, $R^2 = 0.682$) dan SWM ($R = 0.802$, $R^2 = 0.643$). Keputusan pengesahan, R bagi musim NEM dan SWM masing-masing

menunjukkan pekali korelasi yang tinggi, iaitu 0.8035-0.8156 dan 0.8093-0.8178. Juga, untuk kaedah PCR, keputusan penyesuaian terbaik untuk data XCO_2 memberikan nilai pekali penentuan terlaras yang tinggi, iaitu 0.898 dan 0.868 bagi musim NEM dan SWM. Pembolehubah sepunya yang wujud dalam kedua-dua persamaan PCA1 dan PCA2 adalah AOT dan Suhu. Keputusan pengesahan yang diperolehi masing-masing menunjukkan pekali korelasi yang tinggi untuk musim NEM dan SWM, iaitu 0.8584-0.9149 dan 0.8832-0.8944. Nilai RMSE bagi XCO_2 yang diramal menggunakan kaedah MLR untuk kedua-dua musim masing-masing adalah 1.56208 dan 1.71421. Manakala, nilai RMSE bagi XCO_2 yang diramalkan didapati masing masing 0.84924 dan 1.01879 dengan menggunakan kaedah PCR. Nilai statistik diramal and diperolehi dari XCO_2 memiliki kesepakatan yang sangat baik dari segi konsisten dan kebolehpercayaan model ramalan. Daripada keputusan yang diperolehi, kaedah PCR mencapai prestasi yang lebih baik berbanding dengan kaedah MLR untuk meramal nilai XCO_2 di Semenanjung Malaysia. Secara keseluruhan, keputusan ini jelas menunjukkan kelebihan menggunakan data GOSAT satelit dan analisis korelasi untuk mengkaji kesan pembolehubah- pembolehubah atmosfera terhadap XCO_2 di semenanjung Malaysia. Dengan demikian, kita menyimpulkan pendekatan pemodelan ini mempunyai potensi yang besar di kawasan yang lain.

A NEW ALGORITHM FOR ASSESSING THE XCO_2 OVER PENINSULAR MALAYSIA BASED ON GOSAT DATA

ABSTRACT

The increasing carbon dioxide (CO_2) concentration induced by anthropogenic activities has been the focal point of many studies due to the adverse effects of global warming and climate change on the environment. To achieve a healthy environment, studying the transport, distributions and source regions of CO_2 in Malaysia is necessary. The main purpose of this research is to develop an algorithm for calculating the column-averaged dry air mole fraction of carbon dioxide (XCO_2) over Peninsular Malaysia. Four regression algorithms, which are denoted as XCO_2 NEM, XCO_2 SWM, PCA1 (XCO_2 NEM season) and PCA2 (XCO_2 SWM season), were developed using Greenhouse Gases Observing Satellite (GOSAT) data and statistical methods. In addition, this study seeks to analyse and investigate the impacts of selected atmospheric variables with the XCO_2 data. Different statistical analysis methods, including multiple linear regression (MLR) and principal component regression (PCR), were applied to the GOSAT datasets. Additional analysis was conducted in different monsoon seasons to achieve this study's objective. SPSS software was used to test the performance of the MLR and PCR methods in terms of the root-mean-square-error (RMSE). The results showed that the XCO_2 regression equations using the MLR method were highly correlated with atmospheric variables in the NEM ($R= 0.826$, $R^2 = 0.682$) and SWM ($R= 0.802$, $R^2 = 0.643$) seasons. The validation results showed that XCO_2 yielded a strong R^2 for the NEM and SWM seasons, i.e., 0.8035 to 0.8156 and 0.8093 to 0.8178, respectively. Additionally, for the PCR method, the best fit results for the XCO_2 data gave the

high adjusted R^2 coefficients, i.e., 0.898 dan 0.868 for both the NEM and SWM seasons. The common variables that appeared in both the PCA1 and PCA2 equations were the AOT and temperature. The obtained validation results exhibited high coefficients of determination for the NEM and SWM seasons, i.e., 0.8584 to 0.9149 and 0.8832 to 0.8944, respectively. The RMSE for the predicted XCO_2 values using the MLR method were 1.56208 and 1.71421 for the NEM and SWM, respectively, and the corresponding RMSEs were 0.84924 and 1.01879, respectively with PCR method. The predicted and observed XCO_2 values exhibited very good agreement in term of consistency and reliability of the prediction model. The PCR method resulted in better predicted XCO_2 values over peninsular Malaysia than the MLR method. Overall, these results clearly indicate the advantage of using GOSAT data and a correlation analysis to investigate the impact of atmospheric variables on XCO_2 over peninsular Malaysia. Therefore, this modelling approach has great potential in other areas.

CHAPTER 1

INTRODUCTION

1.0 Overview

Since the start of the industrial revolution and economic and social development in the 19th century, the concentration of carbon dioxide (CO_2), which is an atmospheric greenhouse gas, has been steadily rising in the atmosphere primarily due to fossil fuel combustion, land use change, cement production, biomass burning and deforestation, thus perturbing the natural carbon cycle (American Meteorological Society, 2012, Solomon et al., 2007). A greenhouse gas is a gas in an atmosphere that absorbs and emits radiation within the thermal infrared range. This process is the fundamental cause of the greenhouse effect. The primary greenhouse gases in Earth's atmosphere are water vapor, carbon dioxide, methane, nitrous oxide, and ozone. CO_2 has also been recognized as the most important anthropogenic greenhouse gas (GHG), receiving significant attention in the literature (Olivier et al., 2012; Peters et al., 2011).

The increases in CO_2 are leading to a warmer climate with adverse consequences, such as more numerous droughts, storms and floods, melting glaciers and an increase in extreme weather conditions (IPCC 2001, 2007). Statistics have shown that the CO_2 concentration has increased 30% globally, while the temperature has increased by 0.3 – 0.6 °C in recent years (Chakraborty et al., 2000). It is of primary political and scientific concern to estimate the natural and anthropogenic sources and sinks at various spatial and temporal scales. Currently, CO_2 concentrations are mainly measured from ground-based observation platforms

distributed in different areas of the world. Mauna Loa station, which is located on a high volcano in the Hawaii islands, began collection of atmospheric CO_2 concentration observations in 1957 and has revealed evidence of increasing CO_2 (Keeling et al. 1976). However, there are significant gaps and large uncertainties in the sources and sinks of CO_2 (Stephens et al., 2007). The limited spatial coverage and the proximity to local sources and sinks make model estimates susceptible to transport errors, especially for continental regions (Marquis and Tans, 2008). In addition, surface networks are limited in their capability of representing complex atmospheric mixing in the mid- to high troposphere, where the surface signal is diluted (Huntzinger et al., 2012).

Increased attention has been devoted to the application of remote sensing observations for estimating atmospheric CO_2 concentration (Zhang, 2010), and such observations can contain information that is not available from ground-based stations. In addition, the increase spatiotemporal resolution and accuracy of satellite measurements makes remote sensing a practical tool for monitoring CO_2 emissions at regional scales. Currently, the Thermal and Near-infrared Sensor for Carbon Observation Fourier Transform Spectrometer (TANSO-FTS) on board the Greenhouse Gases Observing Satellite (GOSAT), which was launched in January 2009 by the Japan Aerospace Exploration Agency (JAXA), may enhance our understanding of the dynamic processes that influence atmospheric CO_2 concentrations (Rayner and O'Brien, 2001, Houweling et al., 2004). In addition, existing satellites are the only orbiting instruments measuring near-infrared (NIR) radiation with sufficient spectral resolution to retrieve the column-averaged dry air molar fraction of CO_2 (Reuter et al., 2010). These observations offer the possibility

of closing these gaps (Miller et al., 2007, Chevallier et al., 2007). Moreover, prior to 2002, GHG concentrations could not be measured directly using remote sensing techniques.

In Malaysia, industrialization, urbanization and rapid traffic growth have contributed significantly to economic growth. Pockets of heavy pollution are being created by emissions from major industrial zones, increases in the number of motor vehicles and trans-boundary pollution. In addition, Malaysia is located in a humid equatorial region with high temperatures and heavy rainfall (Tangang et al., 2007). Thus, cloudy conditions are an obstacle for acquiring high-resolution and high-quality satellite data. The high resolution that is associated with special satellite specifications is required to study how atmospheric variables affect atmospheric CO_2.

1.1 Problem Statement

Carbon dioxide is the primary anthropogenic GHG and contributes up to 70% of global warming. The increased presence of GHGs in the atmosphere cause major problems and threaten the livelihood of our society. These gases have been associated with climate change, which has influenced land and water resources and food and pasture availability and has caused the disappearance of plants and animal species and loss of habitat.

Over the past few decades, the atmospheric gas abundances have been measured using balloons, aircraft and sparsely distributed measurement sites. These observations have produced important insights into flux variability. However, they lack high-frequency surface observations. *In situ* measurements from the ground, tall

towers and airplanes are very accurate and precise. However, large parts of the Earth, e.g., Southern America, East Asia, Australia and Africa, remain unobserved.

Considering the development of specialized remote sensing CO_2 observations and common research interests, very few long-term studies have been conducted. CO_2 seasonality studies, e.g., the northeast monsoon (NEM) and southwest monsoon (SWM), have primarily encompassed a single year. These monsoons will affect the climate and have different impacts on atmospheric parameters.

Malaysia has very limited atmospheric data from ground stations. Therefore, satellite remote sensing instruments are effective for monitoring the global distributions of atmospheric gases with high spatial and temporal resolutions (Baker et al., 2010). The advantages of constant and real-time observations by remote sensing instruments have been largely ignored, possibly due to the lack of reference data. The TANSO instrument on-board the GOSAT satellite has a high sensitivity down to the Earth's surface, where the sources and sinks of CO_2 are located. This is important for improving our understanding of the sources and sinks of CO_2.

1.2 Scope of the Study

This study mainly focuses on the development of new algorithms for retrieving XCO_2 in peninsular Malaysia. The algorithms were determined via regression analysis using GOSAT satellite data for the period 2009-2012. Multiple linear regression (MLR) and principal component regression (PCR) were utilized to evaluate the effectiveness of the algorithm. In addition, this investigation was also conducted to analyse the effects of atmospheric variables on XCO_2 using various

statistical methods. Finally, a validation was performed for the newly generated XCO_2 algorithm with observed GOSAT and AIRS satellite data.

1.3 Research Objectives

The objectives of this study are as follows:

1. To develop an algorithm of the column-averaged dry air mole fraction of carbon dioxide (XCO_2) over peninsular Malaysia using GOSAT satellite data.
2. To evaluate the effectiveness of the MLR and PCR methods for predicting XCO_2.
3. To investigate and analyse the effects of the atmospheric variables on XCO_2 using various statistical methods.
4. To validate the newly generated XCO_2 algorithm with GOSAT satellite data and AIRS instrument data.

1.4 Novelty of this study

There is no ground truth station for collecting CO_2 data in peninsular Malaysia. Obtaining continuous CO_2 measurements is a very difficult task over the study area. A GOSAT satellite having the capabilities to do CO_2 and CH_4 observations remotely at a good resolution has provided a unique opportunity to understand their distribution. These two gases contribute up to 80% of the anthropogenic global warming. Therefore, information is retrieved from GOSAT and employed to develop an algorithm for predicting XCO_2 via multiple linear regression (MLR). Statistical methods were utilized to analyse the atmospheric data and generate new algorithm for XCO_2. This research work is the first study to use

GOSAT data to analyse the effects of atmospheric parameter's consisting of the aerosol asymmetry factor (AAF), aerosol optical thickness (AOT), temperature (Temperature), water vapor (H_2O vapor) and aerosol single scattering albedo (SSA) on XCO_2 in this region. In addition, a comparative evaluation of XCO_2 modelling using the MLR and PCR methods with the same data has not been conducted in peninsular Malaysia.

1.5 Structure of the Thesis

This thesis consists of five chapters. The first chapter provides the scientific background relevant for the topic of this thesis. A literatures review on detailed descriptions of the GOSAT instrument information and AIRS instrument, the atmosphere, the natural greenhouse effect, global warming and climate change, aerosol optical properties, greenhouse gases and an application of statistical analysis in atmospheric remote sensing were used in this research are presented in chapter two. Chapter three describes the study areas, research materials, software, tools and methodology used for this research. Chapter four presents all of the results of this research and provides a discussion of the processing analyses. This chapter also focuses on the comparison and validation of the XCO_2 algorithms. In addition, statistical methods were used to compare the performance of the MLR method and principal component regression method in predicting XCO_2. Chapter five summarizes the results of this research. Recommendations for future studies are also included in this chapter.

CHAPTER 2

LITERATURE REVIEW

2.0 Introduction

This chapter discusses the descriptions of the GOSAT instrument information and AIRS instrument, the atmosphere, natural greenhouse effect, global warming and climate change, aerosol optical properties and atmospheric GHGs from GOSAT data and a statistical analysis published in a previous work, including their results and how their studies relate to the current study. In addition, the GOSAT instrument is discussed in detail, and a comparison of different retrieval algorithms based on GOSAT spectral data is also provided. The reliability of GOSAT XCO_2 observations is examined based on the calibration and validation work in the literature.

2.1 Introduction to GOSAT

GOSAT was successfully launched on January 23, 2009, from Tanegashima Island, Japan. The spacecraft is the world's only satellite developed jointly by the Japan Aerospace Exploration Agency (JAXA), the Ministry of the Environment, Japan (MOE) and the National Institute for Environmental Studies, Japan (NIES) to measure both the column-averaged dry air mole fraction of CO_2 (XCO_2) and the column-averaged dry air mole fraction of CH_4 (XCH_4), which are the two major anthropogenic greenhouse gases (GHGs).

The objectives of the GOSAT mission are to estimate emissions and absorptions of GHGs on a sub-continental scale with increased accuracy and assist environmental administrations verify the reduced carbon balance of the land ecosystem and make assessments of regional emissions and absorptions (JAXA, 2015). By examining the GOSAT observational data, scientists will be able to improve our understanding of the global composition of greenhouse gases and the effects on global climate change. These new findings will enhance future climate change predictions and can be used to evaluate the impacts.

2.2 GOSAT Instrument and Observation Method

GOSAT, i.e., TANSO's platform, is in a sun-synchronous orbit with a local overpass time of 13:00 and an inclination angle of 98°; thus, the platform can take measurements of the ocean, land, ice, and atmosphere. This environmental satellite flies at an altitude of approximately 666 km and completes one orbital period in approximately 100 minutes (Kuze et al., 2009). The satellite has a three-day repeat cycle and operates on global basis. The schematic diagram of GOSAT is shown in Figure 2.1.

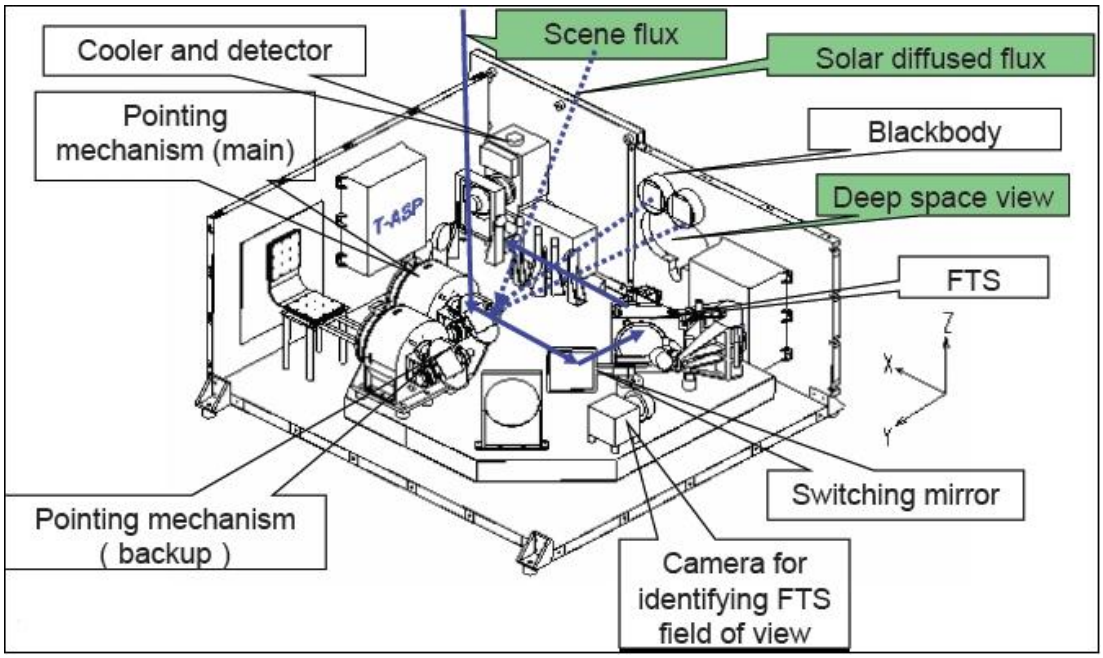

Figure 2.1 Schematic diagram of GOSAT (JAXA, 2015).

The nadir-looking Thermal And Near-infrared Sensor for carbon Observation (TANSO) is the main instrument onboard GOSAT. TANSO consists of two subunits: a Fourier Transform Spectrometer (FTS) and a Cloud and Aerosol Imager (CAI) (Guo et. al, 2012b). TANSO measures surface-reflected sunlight and emitted thermal infrared radiation at wavelengths from 0.76 to 14.3 mm. Tables 2.1 and 2.2 summarize the characteristics and specifications of these two instruments.

Table 2.1 Characteristics and specifications of the TANSO-FTS

	Band 1	**Band 2**	**Band 3**	**Band 4**
Spectral coverage (μm)	0.758-0.775	1.56-1.72	1.92-2.08	5.56-14.3
Spectral resolution (cm^{-1})	0.2	0.2	0.2	0.2
Polarized light observation	Performed	Performed	Performed	Not Performed
Targeted gases	O_2	CO_2,CH_4	CO_2,H_2O	CO_2,CH_4
Angle of instantaneous field of view	15.8 mrad (corresponds to 10.5 km when projected on the Earth's surface)			

Tables 2.2 Characteristics and specifications of the TANSO-CAI

	Band 1	**Band 2**	**Band 3**	**Band 4**
Spectral coverage (μm)	0.370-0.390	0.664-0.684	0.860-0.880	1.56-1.65
Targeted substances	Cloud and aerosol			
Swath (km)	1000	1000	1000	750
Spatial resolution at nadir (km)	0.5	0.5	0.5	1.5

The TANSO-FTS is an optical interference instrument. The TANSO-FTS has three spectral bands (band 1, band 2 and band 3) in the shortwave infrared (SWIR) region that are used to retrieve the XCO_2 and photon path length probability density function (PPDF) (Andrey et al., 2012). For the SWIR bands, solar light is split into two orthogonally polarized beams (P and S components) with different optical paths. The solar light in band 4 is not split. The TANSO-FTS instantaneous field of view is 15.8 m rad, which corresponds to a nadir footprint diameter of approximately 10.5 km. The pointing mechanism of the TANSO-FTS enables off-nadir observations. Because of the limited driving angles of the pointing mirror (±35° in the cross-track direction and ±20° in the along-track direction), GOSAT performs sun-glint measurements within narrow (~30°) near-equator latitude ranges. Fourier transforms are performed to obtain the spectral information. More details on the TANSO-FTS can be found in Kuze et al. (2009).

The TANSO-CAI is designed not only to determine whether images are cloud/aerosol free but also to estimate and correct for the effects of clouds and aerosols on the spectra obtained by the FTS. The image data from the CAI are used to examine the existence of clouds over extended areas that encompass the FTS's

field of view (FOV). Because the FOV detects both clouds and aerosols, the characteristics of cloud and aerosol amounts can be measured. The CAI is a great tool to map the state of the Earth's surface and the atmosphere during the daytime. The sensor is also designed with 4 bands at wavelengths of 0.37-0.39 μm, 0.664-0.684 μm, 0.86-0.88 μm and 1.56-1.65 μm, respectively. The spatial resolution of the CAI is up to 0.5 km for the first 3 bands and 1.5 km for band 4.

The FTS takes three day to cover the entire globe, capturing fifty-six thousand measurements in the process. However, only two to five per cent of the collected data are usable for calculating column abundances of CO_2 and CH_4 due to limited areas under clear sky conditions. Despite this fact, the number of data points significantly surpasses the current number of ground monitoring stations, which are approximately 200. GOSAT aids in filling in the ground observation network gaps.

2.3 GOSAT Data Products

The satellite data from GOSAT are obtained from the National Institute for Environmental Studies (NIES) of Japan. GOSAT data products contain level 1, level 2, level 3, and level 4. The Level 1 data (FTS Level 1B, CAI Level 1B, and CAI Level 1B+ data) contain spectra and radiances acquired by the satellite. The higher-level data products (FTS Level 2, CAI Level 2, FTS Level 3, CAI Level 3, Level 4A, and Level 4B data products) store the column abundances of CO_2 and CH_4 retrieved from the radiance spectra in band 1, band 2 and band 3 of the FTS.

The Japan Aerospace eXploration Agency (JAXA) is responsible for processing Level 1A/1B data obtained by the FTS and Level 1A from the CAI; they

transfer these products to the GOSAT Data Handling Facility (GOSAT DHF) at the National Institute for Environmental Studies (NIES). There are three types of GOSAT products, i.e., “Standard” for general users, “Research” for registered researchers and “Internal” for restricted users (Masataka et al., 2014). Table 2.3 lists all GOSAT data product types. All of these data are distributed through the GOSAT User Interface Gateway (GUIG), which is the GOSAT data product distribution site (Watanabe et al., 2011).

Table 2.3 List of GOSAT data products (Masataka et al., 2014)

Level	Sensor	Product Name	Category	Dist. Unit	Format
L1A	FTS	FTS L1A data	Internal	FTS scene	HDF5
	CAI	CAI L1A data	Internal	CAI scene	
L1B	FTS	FTS L1B data	Standard	FTS scene	
	CAI	CAI L1B data	Standard	CAI frame	
L1B+	CAI	CAI L1B+ data	Standard		
L2	FTS SWIR	L2 CO_2 column amount (SWIR)	Standard	multiple scans in a FTS scene	
		L2 CH_4 column amount (SWIR)	Standard		
		L2 H_2O column amount (SWIR)	Research		
	FTS TIR	L2 CO_2 profile (TIR)	Standard		
		L2 CH_4 profile (TIR)	Standard		
		L2 temperature profile (TIR)	Research		
		L2 H_2O profile (TIR)	Research		
		L2 H_2O column amount (TIR)	Research		
	CAI	L2 cloud flag	Standard	CAI frame	
		L2 cloud property	Research		
		L2 aerosol property	Research		
L3	FTS SWIR	L3 global CO_2 distribution (SWIR)	Standard	global, monthly	
		L3 global CH_4 distribution (SWIR)	Standard		
	FTS TIR	L3 global CO_2 distribution (TIR)	Standard		
		L3 global CH_4 distribution (TIR)	Standard		
	CAI	L3 global radiance distribution	Standard	global, daily	
		L3 global reflectance distribution	Standard		
		L3 global cloud property	Research	global, every 3 days with the accumulated data for 30 days	
		L3 global aerosol property	Research		
		L3 NDVI	Standard	regional, every 3 days with the accumulated data for 30 days (30 deg. Lat by 60 deg. Lon)	
L4A	—	L4A global CO_2 flux	Standard	global, anual (64 regions for Text, 1 deg. mesh for Net CDF)	Text and Net CDF
		L4A global CH_4 flux	Standard	global, anual (43 regions for Text, 1 deg. mesh for Net CDF)	
L4B	—	L4B global CO_2 distribution	Standard	global, monthly (2.5 deg. mesh)	Net CDF
		L4B global CH_4 distribution	Standard		

The FTS Level 1B data contain the radiance spectra, which are obtained during 1/60 of an orbital revolution using a Fourier transformation. The CAI Level 1B data are pixel-scale radiances, which are converted from the digital counts of the CAI by multiplying by the given calibration factors. The CAI Level 1B+ data use the same Level 1B radiance data from the FTS; the geographical locations of individual pixel images are corrected for skewness induced by topographical roughness of the ground surface and are projected using an interpolation method to produce a map. The FTS Level 1B data contain the radiance spectra, which are obtained during 1/60 of an orbital revolution using a Fourier transformation. The CAI Level 1B data are pixel-scale radiances, which are converted from the digital counts of the CAI by multiplying by the given calibration factors. The CAI Level 1B+ data use the same Level 1B radiance data from the FTS; the geographical locations of individual pixel images are corrected for skewness induced by topographical roughness of the ground surface and are projected using an interpolation method to produce a map.

The FTS SWIR Level 2 data products store the column abundances of CO_2 and CH_4 retrieved from the radiance spectra in bands 1 through 3 of the FTS. There are three types of FTS SWIR Level 2 products, i.e., “L2 CO_2 column amount (SWIR)” and “L2 CH_4 column amount (SWIR)”, which are categorized as “Standard” and “L2 H_2O column amount (SWIR)” in research projects. The FTS TIR Level 2 data products are vertical concentration profiles of CO_2 and CH_4 derived from the radiance spectra in band 4 of the FTS. There are two types of FTS TIR L2 products, i.e., “L2 CO_2 profile (TIR)” and “L2 CH_4 profile (TIR)”, which are stored as HDF files. The CO_2 or CH_4 concentration data are stored at the average pressure level of

each retrieval grid layer. There are 27 and 22 retrieval grid layers for CO_2 and CH_4, respectively. The Level 2 cloud flag data product stores the clear-sky confidence levels calculated from the CAI Level 1B data.

The FTS SWIR Level 3 data products store the monthly global distributions of CO_2 and CH_4 obtained from the FTS SWIR Level 2 column-averaged dry air mole fraction of CO_2 and CH_4. A geostatistical calculation technique called ordinary kriging method is applied to estimate values in blank regions of the FTS SWIR Level 2 distributions. The ordinary kriging method predicts the observed value of an arbitrary point on this random field, the characteristics of which are a function of the statistical properties of the observational data. The Level 3 product can be generated on a monthly basis by estimating global semi-variogram curves from the Level 2 products for each month and interpolating spatially within a region with a radius of 1000 km from existing Level 2 data locations. All values are gridded into 2.5º cells. The FTS TIR Level 3 data products are global maps of CO_2 and CH_4 at different pressure levels and are processed following the same procedures discussed above. These data products can be used to illustrate the global spatial variations of greenhouse gases.The CAI Level 3 radiance distribution data products collected during the three-day cycle are assemble to provide a global cloud distribution map. The CAI Level 3 global reflectance distribution data product includes global ground surface characteristics. These data are processed by choosing the clear-sky images from the CAI data compiled over a month and synthesizing them on a global distribution map. The Level 3 normalized difference vegetation index (NDVI) data are generated via the divergence of the CAI radiances in band 3, which are sensitive to vegetation, whereas band 2 is less sensitive to vegetation.

The Level 4A data product includes monthly CO_2 fluxes in 64 global regions that are inversely determined from the FTS SWIR Level 2 column-averaged mixing ratios and ground-based observational data using a global atmospheric transport model provided by the US NOAA Earth System Research Laboratory. Details of the data processing algorithms and descriptions of the a priori flux datasets are presented in Maksyutov et al., (2013). The Level 4B data product includes three-dimensional global CO_2 concentrations in three dimensions calculated from the Level 4A data product using the atmospheric transport model. The data product has a horizontal resolution of 2.5°×2.5° and six-hour intervals.

2.4 Validation of the GOSAT Data Products

For the GOSAT data products to be used in the science community, the precision and bias of the data products must be clarified and validated. The GOSAT data validation team uses high-precision reference data acquired by ground-based high-resolution Fourier transform spectrometers in the Total Carbon Column Observing Network, (TCCON), which operate independently, and airborne measurements to validate the GOSAT FTS SWIR Level 2 data products. The bias and standard deviation for XCO_2 and XCH_4 are less than 1%. The period of validation was from June 2009 to November 2012 (Masataka et al., 2013). Cloud and aerosol properties are also validated using the data obtained by remote sensing instruments, such as ground-based sky radiometers and lidars.

Data collected by aircraft from Japan Airlines that participate in the Comprehensive Observation Network for Trace gases by Airliner (CONTRAIL)

project and the US National Oceanic and Atmospheric Administration's airborne measurement program are used. The results of the comparison indicate that the retrieved Level 2 CO_2 and CH_4 column abundances are broadly consistent with the reference values (JAXA, 2015).

2.5 Atmospheric Infrared Sounder (AIRS)

The Atmospheric Infrared Sounder (AIRS) is one of several instruments onboard the Earth Observing System (EOS) Aqua satellite, which was launched on 4 May 2002 (Figure 2.2). The Aqua satellite is in polar sun-synchronous orbit, flying at an altitude of approximately 705 km and completing an orbital cycle in 98.8 minutes. The platform's equatorial crossing is at 13:30 local time; the cycle period is 16 days (Aumann et al., 2003).

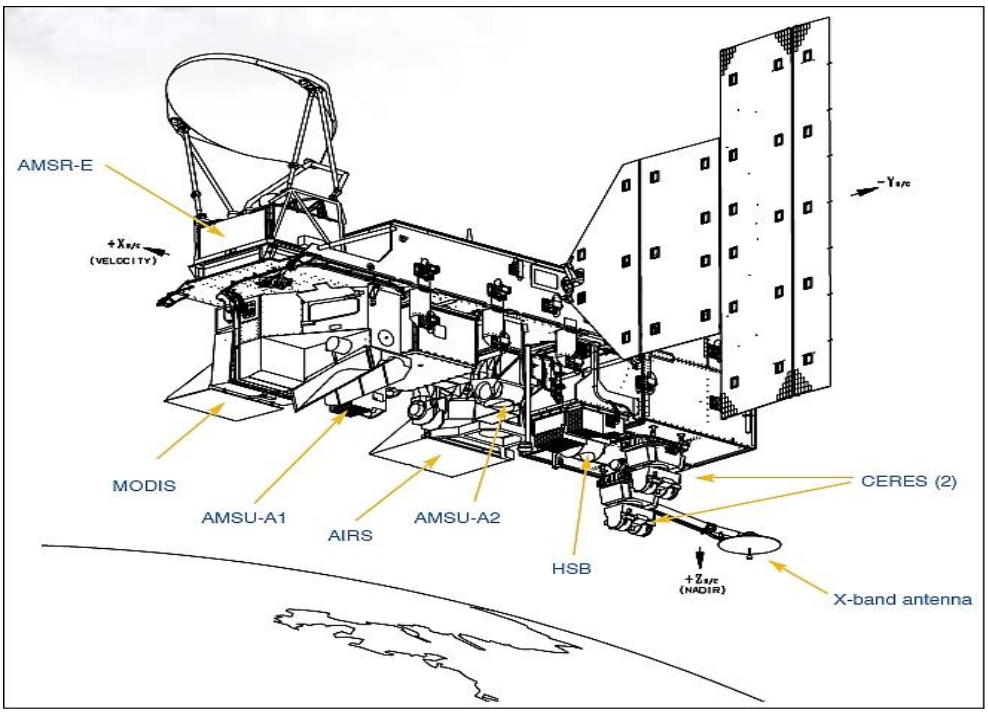

Figure 2.2 Schematic diagram of Aqua satellite (NASA, 2015).

The AIRS instrument includes two companion microwave instruments, i.e., the Advanced Microwave Sounding Unit (AMSU) and the Humidity Sounder for Brazil (HSB). The AIRS/AMSU/HSB combination provides coincident observations of the Earth's atmospheric, land and ocean surface temperatures, and greenhouse gases for analysing several interdisciplinary issues in the earth sciences. The AIRS channels consist of spectral features that indicate several anthropogenic greenhouse gases, including CO_2, CH_4, and CO (Haskins and Kaplan, 1992). Table 2.4 shows the AIRS technological specifications.

Table 2.4 AIRS technology specifications (Fishbein et al., 2007)

Instrument	AIRS
Size	Stowed: 116.5 × 80 × 95.3 cm Earth shade deployed: 116.5 × 158.7 × 95.3 cm
Spectral Range	IR: 3.74 – 15.4 μm, 2378 channels with $\lambda/\Delta\lambda$= 1200 resolution VIS/NIR: 0.4 – 1.1 μm with 4 channels
Instrument Field of View	IR: 1.1 º (13.5 km at nadir from 705 km altitude) VIS/NIR: 0.2 degree (2.3 km from 705 km altitude)
Mass / Power	177 kg / 22o Watt
Aperture	IR: 10 cm; VIS/NIR: 0.2 to 1 cm
Swath Width	99 degree (1650 km from 705 orbit altitude)
Scan Sampling	IR: 90 × 1× 1.1 º; VIS/NIR: 720 × 8 × 0.2 º
Spatial Coverage	Scan Angle: +/- 49.5 around nadir IFOV: 0.185
Ground Coverage	+/- 49.5 degrees around nadir
Ground Footprint	90 per scan, 22.4 ms footprint
Temporal Coverage	Global, twice daily swath (daytime and night-time)
Spectral Resolution	13.5 × 13.5 km in the nadir
Radiometric Calibration	+/- 3% absolute error

2.6 The Atmosphere

The atmosphere is a gaseous shell surrounding the planet that is retained by gravitational attraction. The atmosphere protects life on Earth by interacting with

incoming ultraviolet solar radiation. In these processes, the constituents and the structure of the atmosphere play an essential role. For more detailed information can be found in Roedel (2000) and Burrows et al. (2011).

2.6.1 Constituents of Atmosphere

The Earth's atmosphere is mainly composed of nitrogen (N_2) and oxygen (O_2), which constitute 78% and 21% of the volume of air, respectively. The remaining 1% is composed of trace gases, including argon (Ar), helium (He), carbon dioxide (CO_2), methane (CH_4), nitrous oxide (N_2O), water vapor (H_2O vapor), and ozone (O_3) (Lutgens et al., 2006). The main components, chemical notations and their concentrations in dry air are listed in Table 2.5. The concentrations are given in percentage (%), ppmv (parts per million by volume) and ppbv (parts per billion by volume). Almost all of these gases are involved in important chemical and physical processes that occur in the atmosphere.

Table 2.5 Main atmospheric components and their concentration in dry air (Burrows et al., 2011).

Component	**Chemical Notation**	**Volume Fraction in Air**
Nitrogen	N_2	78.084 %
Oxygen	O_2	20.948 %
Argon	Ar	0.923 %
Carbon Dioxide	CO_2	390 ppmv
Helium	He	5.24 ppmv
Methane	CH_4	1.9 ppmv
Molecular Hydrogen	H_2	0.55 ppmv
Nitrous Oxide	N_2O	0.31 ppmv
Carbon Monoxide	CO	50-250 ppbv
Ozone (Tropospheric)	O_3	10-500 ppbv

Ozone (Stratospheric)	O_3	0.5-10 ppmv

2.6.2 Structure of the Atmosphere

The atmosphere is divided into four distinct layers based on substantial changes in temperature (Figure 2.3). These layers are characterized in terms of their specific vertical temperature gradients (Dubin et al., 1976). The troposphere is the lowest layer of atmosphere, extending from the Earth's surface to a height of approximately 18 km in the tropics, 12 km at mid-latitudes and 6 – 8 km near the poles. The temperature decreases by 6.5 °C for every kilometre above the Earth's surface. This temperature is achieved by the greenhouse effect, which is described in the next section. Thus, the lowest part of the troposphere, the planetary boundary layer, is typically the warmest section of the troposphere. Most of the atmospheric water vapor is located in this layer; thus, it is the layer where most of Earth's weather occurs. The tropopause is located at the top of the troposphere and separates the troposphere from the stratosphere at a height of approximately 50 km. The temperature remains fairly constant over this region.

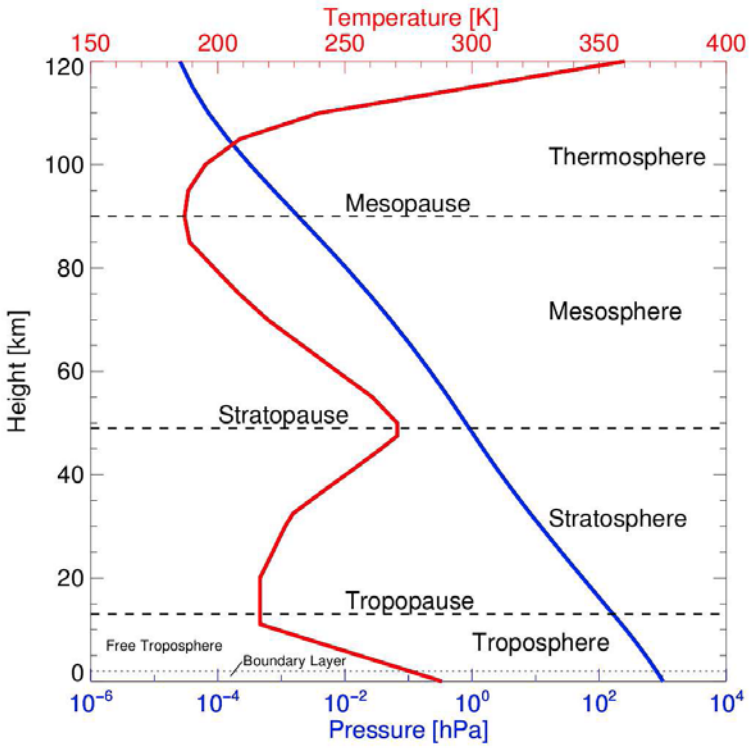

Figure 2.3 Temperature (red) and pressure (blue) profile according to the U.S. standard atmosphere (Dubin et al., 1976).

The stratosphere is located at a height of 12-50 km. Approximately 90% of the ozone in Earth's atmosphere is contained in the stratosphere. The temperature increases with height due to the absorption of ultraviolet (UV) radiation from the sun. The stratopause is the upper boundary of the stratosphere. The mesosphere, or the middle layer, exists above the stratosphere. This is the coldest region of the atmosphere. This layer protects the Earth from meteoroids. At approximately 50 km above the mesosphere, the thermosphere begins. The temperature is very high in this layer due to the absorption of high-energy radiation, which is converted into heat. The change to interplanetary space is called the exosphere and is located at a height of approximately 1,000 km.

2.6.3 The Natural Greenhouse Effect

The greenhouse effect, which is responsible for a warming of the Earth's surface and the lower atmosphere, is a natural process and makes life possible on Earth. The first step in the initiation of the greenhouse effect is a heating of the Earth's surface by the sun. This heating is achieved by the incoming solar energy, which can be characterized by the solar constant. This constant is the amount of solar energy reaching the top of the Earth's atmosphere each second on an area of one square meter perpendicular to the sun direction and is about 1,368 W/m^2. The average of this value over the entire earth is 342 W/m^2 (considering the curvature of the Earth's surface).

As shown in Figure 2.4, two-thirds of the incoming solar energy is absorbed by the surface and the atmosphere. The remaining one-third is reflected back to space. To achieve an energy balance, the absorbed incoming energy is re-emitted back to space. The maximum amount of re-emitted radiation is in longer wavelengths, primarily the infrared spectral region, because the Earth is much colder than the Sun. Both the land and ocean emit plenty of thermal radiation that is absorbed by the greenhouse gases and clouds; some of this radiation is re-radiated back toward the Earth's surface, warming it. The most important greenhouse gas is H_2O vapor, CO_2 is the second most important greenhouse gas.

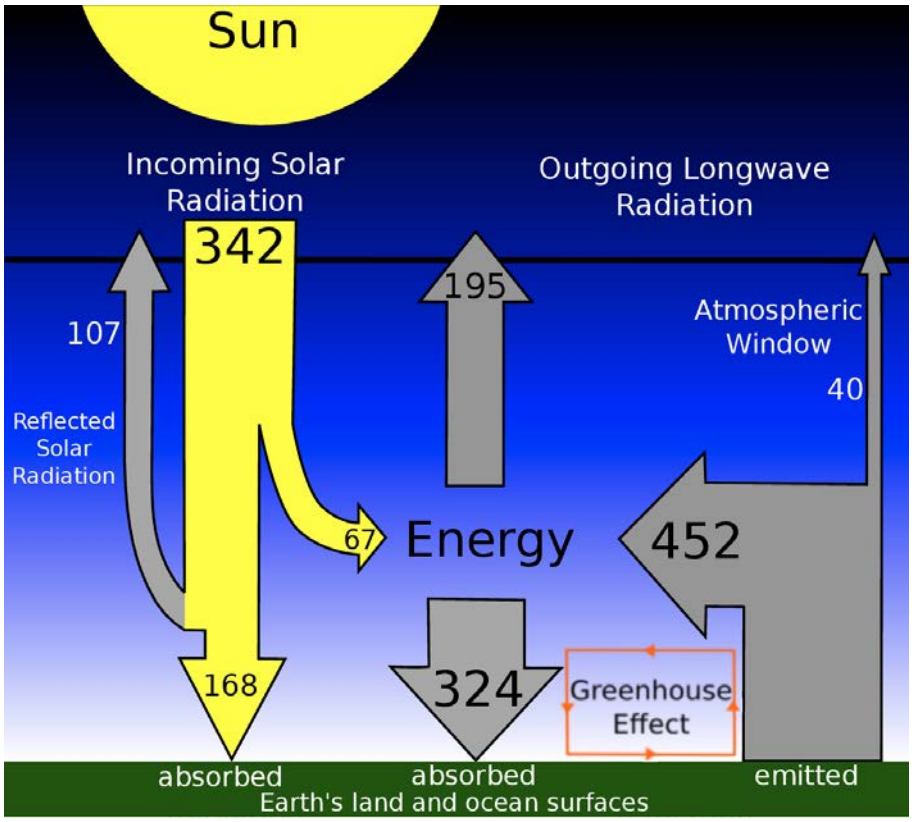

Figure 2.4 Earth's estimated energy balance; all values are given in watts per square meter (Solomon et al., 2007).

The GHGs include O_3, N_2O and CH_4 also contribute to the greenhouse effect (Roedel, 2000). Other important contributors to the greenhouse effect are clouds and aerosols. Without the natural greenhouse effect, the average temperature at the Earth's surface would be below the freezing point of water. Thus, Earth's natural greenhouse effect preserves life on Earth. However, human activities, primarily the burning of fossil fuels and the clearing of forests, causes an amplification of the natural greenhouse effect and leads to global warming with adverse consequences for the Earth (Solomon et al., 2007). More details on the anthropogenic greenhouse effect, global warming and the resulting climate change are given in the next section.

2.7 Global Warming and Climate Change

Global warming and climate change have been occurring for years, and this issue is the focus of public interest. The influence of humans on global warming and climate change is clear; anthropogenic greenhouse gases have reached their highest concentrations in history. As reported by the Fifth Assessment Report of the Intergovernmental Panel on Climate Change (IPCC), “natural and anthropogenic substances and processes that alter the Earth’s energy budget are the drivers of climate change” (IPCC 2013).

In this context, the term “climate change” is the change in climate over time, which can be due to natural variability or human activities (American Meteorological Society, 2012, Denman et al., 2007). The global temperature of the Earth has increased by 0.8 degrees in the last century, with more than half of the increase occurring in the last thirty years (Blunden and Arndt, 2012). Analysis has shown that there is a 95% probability that this warming is attributed to an enhanced greenhouse effect caused by increased greenhouse gas concentrations within the atmosphere (Berger, 2000).

The increasing concentrations of greenhouse gases have a positive impact on radiative forcing, which warms the climate. Radiative forcing is a measure of the effect that a factor has on the balance of outgoing and incoming energy in the Earth’s atmosphere system and indicates the significance of a particular factor as a potential climate change mechanism. A positive radiative forcing causes a warming of the Earth’s atmosphere, whereas a negative radiative forcing results in a cooling effect. Figure 2.5 shows the major radiative forcings for the period 1750–2011. In this report, a level of confidence is expressed using five qualifiers: very low, low,

medium, high, and very high. For given evidence and agreement statement, different confidence levels can be assigned, but increasing levels of evidence and degrees of agreement are correlated with increasing confidence.

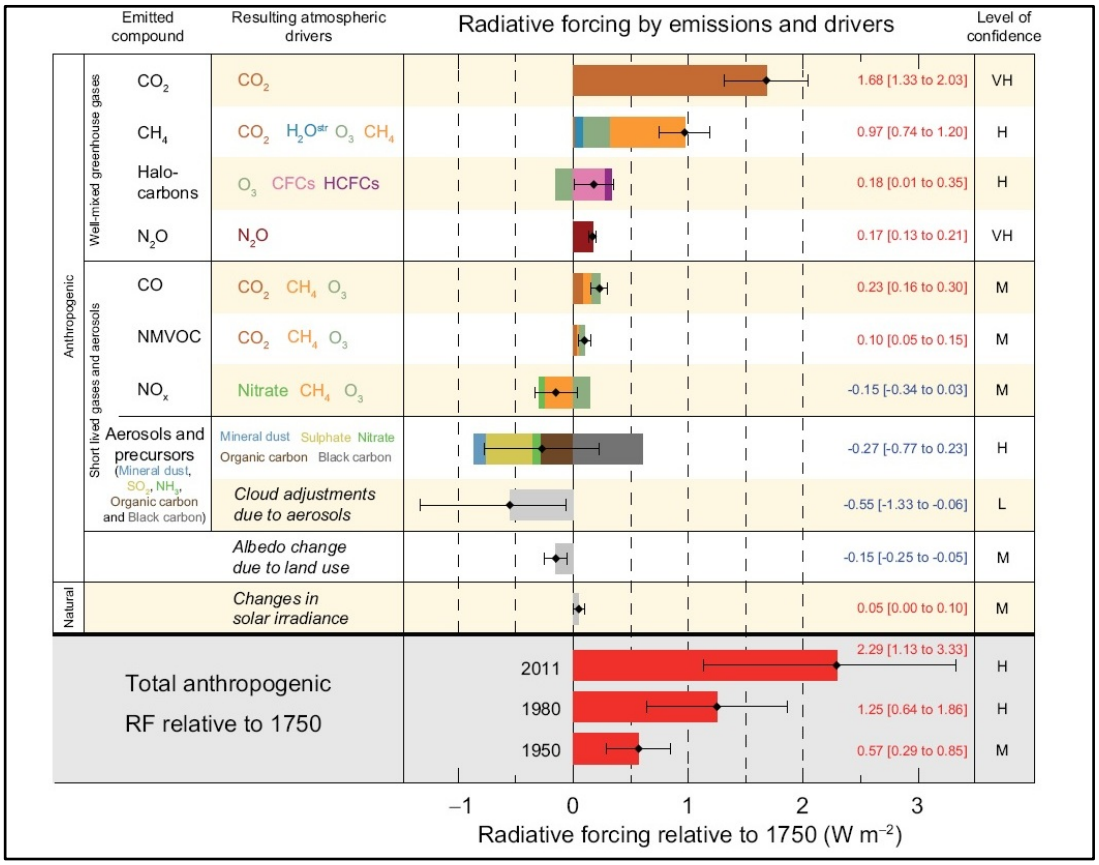

Figure 2.5: Radiative forcing and their uncertainty estimates in 2011 relative to 1750. The forcing are divided into anthropogenic and natural forcing with the Level of confidence (IPCC, 2013)

The radiative forcing for well-mixed greenhouse gases (CO_2, CH_4, N_2O, and halocarbons) from 1750 to 2011 is 3.00 [2.22 to 3.78] Wm^{-2}. The primary anthropogenic greenhouse gas (CO_2) exhibits the largest radiative forcing, i.e., 1.68 [1.33 to 2.03] Wm^{-2}. The increased atmospheric CO_2 concentration has been mainly due to fossil fuel combustion, cement production and deforestation. CH_4 contributes a forcing of 0.97 [0.74 to 1.20] Wm^{-2}, primarily due to agriculture, natural gas